IEEE Photonics Journal
An IEEE Photonics Society Publication

Open Access

Single-Photon Reflectivity and Depth Imaging by Continuous Measurement of Arrival Time of Photons

Volume 11, Number 6, December 2019

Qiurong Yan
Dan Li
Yifan Wang
Yibing Yang
Linao Tang
Yuhao Wang

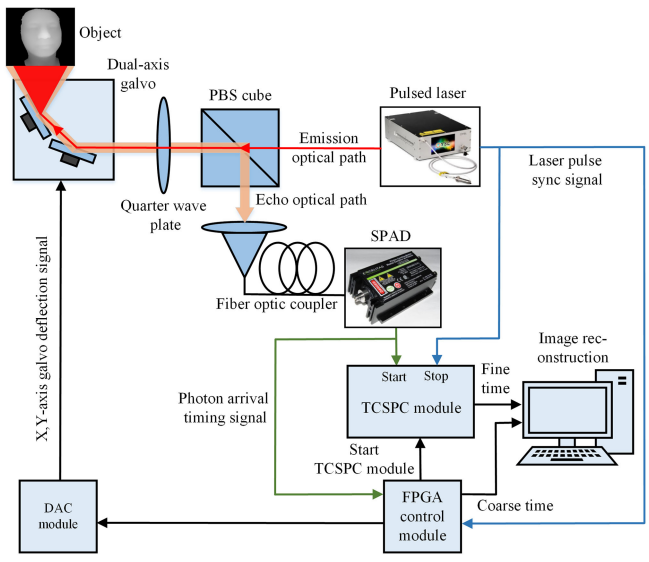

DOI: 10.1109/JPHOT.2019.2945989

Single-Photon Reflectivity and Depth Imaging by Continuous Measurement of Arrival Time of Photons

Qiurong Yan,[1] **Dan Li**,[1] **Yifan Wang**,[1] **Yibing Yang**,[1] **Linao Tang**,[2] **and Yuhao Wang** [1]

[1]Department of Electronics Information Engineering, Nanchang University, Nanchang 330031, China
[2]State Key Laboratory of Transient Optics and Photonics, Xi'an Institute of Optics and Precision Mechanics, Chinese Academy of Sciences, Xi'an 710119, China

DOI:10.1109/JPHOT.2019.2945989
This work is licensed under a Creative Commons Attribution 4.0 License. For more information, see https://creativecommons.org/licenses/by/4.0/

Manuscript received September 25, 2019; accepted October 3, 2019. Date of publication October 11, 2019; date of current version November 12, 2019. This work was supported in part by the National Natural Science Foundation of China under Grants 61865010 and 61565012, in part by the China Postdoctoral Science Foundation under Grant 2015T80691, in part by the Science and Technology Plan Project of Jiangxi Province under Grant 20151BBE50092, and in part by the Funding Scheme to Outstanding Young Talents of Jiangxi Province under Grant 20171BCB23007. Corresponding author: Qiurong Yan (e-mail: yanqiurong@ncu.edu.cn).

Abstract: We demonstrate a reflectivity and depth imaging Lidar system based on a novel photon arrival time measurement method. In this method, the arrival time of photons in a scanning position is continuously measured with a common starting point. The number of laser pulses is counted by a specially designed field programmable gate array (FPGA) control module as the coarse time of arrival photon. Time interval between arrival photon and the nearest coming laser pulse is measured by a time-correlated single-photon counting (TCSPC) module as the fine time of arrival photon. Using the system, not only the single-photon counting imaging can be realized, but also the first photon imaging, the first two photons imaging, etc. can be realized. A photon statistical model based on the doubly stochastic Poisson point processes, a time-gated filtering algorithm, and the reflectivity algorithm based on maximum likelihood estimation are derived. High-sensitivity reflectivity and depth imaging with a resolution of 512 $\times$ 512 pixels are achieved. The experimental results show that the horizontal spatial resolution is 2 mm, the vertical depth resolution is 5.375 cm, and the average number of photons per pixel is less than 1.3 photons.

Index Terms: Lidar, First photon imaging, TCSPC, Reflectivity and depth imaging.

1. Introduction

Single-photon counting Lidar has become a research hotspot for a number of remote sensing applications in recent years [1], [2]. The single-photon counting Lidar comprised a high repetition rate pulsed laser and a single-photon detector [3]–[5]. The reflection intensity and depth of the surface of the long-distance object can be recovered by counting the number of photons in the laser echo signals and measuring time-of-flight (TOF) of the photons [6]. In contrast to analogue optical detector, the timing resolution of single-photon detector is not limited by the duration or rise time of voltage pulse but is determined by the timing jitter of single-photon pulse. Therefore, the single-photon counting Lidar has a higher depth resolution. In addition, due to the use of high sensitivity single photon detectors, remote detection can be achieved with a low-power semiconductor laser.

A Lidar based on a combination of a single-photon detector and a low power semiconductor laser can satisfy the detection of long-range objects in the atmospheric environment [7], [8] and airborne remote sensing [9] with strict limits on weight, size and volume.

Time-correlated single-photon counting (TCSPC) [10]–[13] is a statistical sampling technique applied to detect extremely weak signals. When a photon is detected, the time interval between the single-photon pulse and the laser sync pulse is measured, and a "1" is added in a memory location with an address proportional to the period of the laser sync pulse. After enough measurements, the waveform of light intensity can be constructed using the photon counting histogram in the memory. Poisson noise can be effectively reduced by multiple measurements, so TCSPC technique has higher sensitivity than other photon counting techniques such as gate counting [14] and multi-channel scanning [15], and has been widely used in fluorescence lifetime imaging microscope with picosecond time resolution [16], [17]. To achieve longer range detection, more and more literature reports on the use of TCSPC technique to record TOF of photons and echo pulses in Lidar system [18]–[20]. In 2013, A. McCarthy *et al.* built a Lidar system using a pulsed laser, a gated InGaAs/InP single-photon detector and a TCSPC module. Working at a safe power of the human eye, the depth of the object is obtained by the cross-correlation between the photon impulse response and the photon histogram, and the reflectivity of the object is obtained by the maximum likelihood estimation. The system achieved depth imaging with a resolution of centimeter level [21]. In 2017, A. M. Pawlikowska *et al.* proposed a high-resolution 3D imaging system using a pulsed laser with a wavelength of 1550 nm and an InGaAs/InP single-photon detector. The system uses TOF-TCSPC technique and Alternating Direction Method of Multipliers (ADMM) based Total Variation (TV) algorithm to achieve depth imaging of objects in the range of 800 m to 10.5 km [22]. In 2018, Y. Kang *et al.* combined a pulsed laser with a TCSPC module to demonstrate a fast long-range photon counting depth imaging system. The system realizes depth imaging of objects in the distance of 900 meters, and uses a total variation regularization algorithm for the optimal initial value, which extremely reduces the image processing time of the system [23]. TCSPC uses time-amplitude converter and analog-to-digital converter (TAC-ADC) or time-to-digital converter (TDC) to measure time interval with a high accuracy, but the measurement range is limited. Accurate measurement of long-range TOF of photons require additional assistive techniques [24].

In 2014, A. Kirmani *et al.* proposed a 'first-photon imaging' method. Laser pulses are continuously transmitted to the pixel unit at the scanning position until the first reflected single-photon is detected, and then the next scanning position is performed. The intensity of the light at the scanning point is detected by recording the number of laser pulses that have been emitted. The reflectivity and 3D structure of objects are recovered by exploited the spatial correlations of the real-world scene [25], [26]. Although the first-photon imaging is verified to be suitable for extremely weak luminous flux conditions, the scanning control is more complicated because the measurement time per pixel is not fixed.

This paper presents a continuous, high-precision method for measuring arrival time of photons with a common starting point in a scanning position. In this method, the number of laser pulses is counted by a field programmable gate array (FPGA) control module as the coarse time of arrival photon. Time interval between arrival photon and the nearest coming laser pulse is measured by a TCSPC module as the fine time of arrival photon. Using the system, single-photon counting imaging of the long-range object can be achieved, and the first photon imaging, the first two photons imaging, etc. can be also realized.

2. System Design and Implementation

2.1 Experimental Hardware

Single-photon reflectivity and depth imaging experiment system is shown in Fig. 1. It mainly includes a pulsed laser (Anyang laser SC-PRO), a single-photon avalanche diode (SPAD) detector (EXCELITAS SPCM-AQRH-14-FC32497), a dual-axis galvo (THORLABS GVS002), a TCSPC module (Becker & Hickl GmbH SPC-130), a digital-to-analog converter (DAC) module and an FPGA

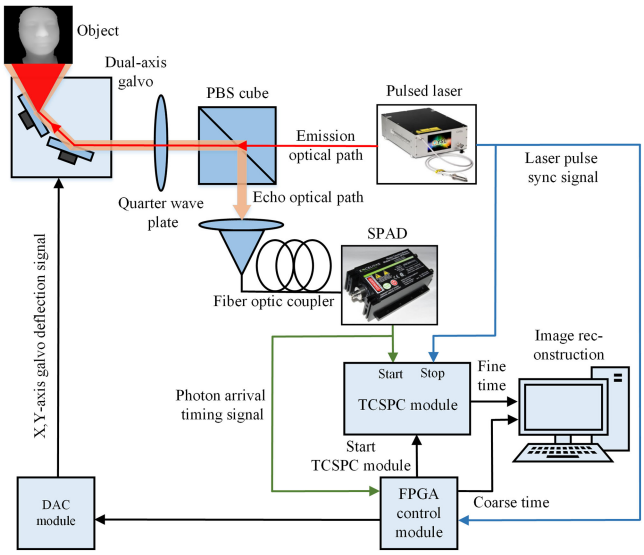

Fig. 1. Schematic diagram of single-photon reflectivity and depth imaging experiment system.

control module. The pulse width of the pulsed laser is 100 ps, the spectral range is 400–2400 nm, and the repetition frequency can be set from 0.1 to 25 MHz. The diameter of laser spot is 2 mm, and laser spot divergence angle is less than 1 mrad. The diameter of active area of the SPAD detector is 180 μm, the photon detection efficiency is 70% at 700 nm, the single-photon timing resolution is 350 ps, the wavelength range is 400–1060 nm, and the dark count rate is less than 100 cps. The TCSPC module has a time resolution of 8 ps, a maximum time bins of 4096.

In order to reduce the interference of stray light and improve the sensitivity of the system, the system adopts the emission-echo common optical path design based on a polarizing beam splitter (PBS) cube and a quarter wave plate [27]. As shown in Fig. 1, in the emission optical path, the laser pulse emitted by the pulsed laser passes through a PBS cube (THORLABS PBS122 with a wavelength range is 620–1000 nm, transmission efficiency $>$90%, reflection efficiency $>$99.5% and a size is 0.5in), then it is split into a reflected S-line polarized laser pulse and a transmitted P-line polarized laser pulse. The P-line polarized laser pulse becomes a circularly polarized laser pulse after passing through the quarter wave plate (CASTECH M5374-1 with a wavelength range is 400-800 nm). Then the circularly polarized laser pulse is reflected to object through the dual-axis galvo. In the echo optical path, the circularly polarized laser pulse is reflected by the object at first, then passes through the dual-axis galvo and the quarter wave plate, and finally becomes a linearly polarized laser pulse. Because of the linearly polarized light beam passes through a quarter wave plate twice, it is still a linearly polarized light beam, but the polarization direction changes by 90° [28]. So the circularly polarized laser pulse is converted into an S-line polarized laser pulse. The S-line polarized laser pulse does not return to the pulsed laser after passing through the PBS cube. Instead, it is reflected into a fiber optic coupler and then enter the SPAD detector. After receiving the echo optical signals, the SPAD detector exports a discrete single-photon pulse sequence, that is, photon arrival timing signal [29], to the FPGA control module and the start input of TCSPC module, and each pulse represents a detected photon. The laser pulse sync signal is input to the FPGA control module and the stop input of TCSPC module. When a single-photon pulse arrive, number of laser pulses is counted by the FPGA control module as the coarse time of arrival photon. Time interval between arrival photon and the nearest coming laser pulse is measured by the TCSPC module as the fine time of arrival photon. In order to achieve 2D scanning of the object, the pulsed laser, the dual-axis galvo and the TCSPC module need to be synchronized under the control of the FPGA control module. Data of the arrival times of photon sequence are output to PC to reconstruct the reflectivity and depth images of the 3D objects.

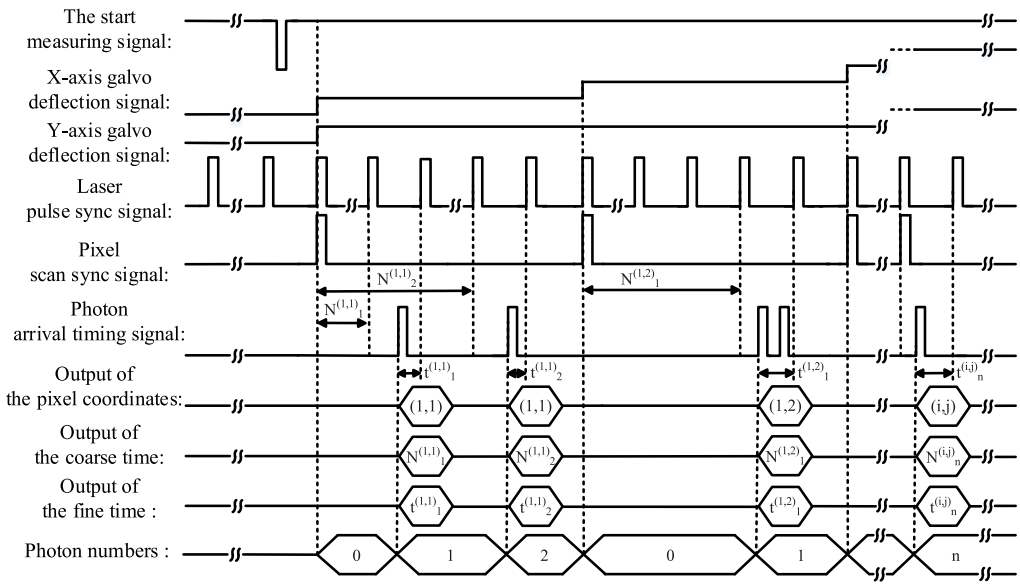

Fig. 2. Timing diagram of FPGA control module.

2.2 Timing of FPGA Control Module

The FPGA control module is designed to control the dual-axis galvo to scan the object, and synchronously record the coarse times and pixels of arrival photons. The timing diagram of the FPGA control module is shown in Fig. 2. When the FPGA control module is used for single-photon counting image, the start measuring signal can be generated by a manual trigger or an external trigger. Laser pulse sync signal with period of T_{laser} is from the pulsed laser. When the falling edge of the start measuring signal is received, the rising edge of the subsequent first arriving of the laser pulse sync signal can be detected. When the rising edge of the laser pulse sync signal is detected, a pixel scan sync signal begins to be generated synchronously by count the laser pulse sync signal. The time interval T_{pix} of adjacent pulses in pixel scan sync signal, controlled by count value of the laser pulse sync signal, represents the dwell time of scanning one pixel. When the rising edge of the pixel scan sync signal is detected, the X-axis galvo deflection signal and the Y-axis galvo deflection signal are synchronously output to dual-axis galvo to let the laser pulses reach the specified scan pixel. The rising edge of the pixel scan sync signal acts as a common starting point for all arrival photons in a scanning pixel. When rising edge of the pixel scan sync signal is received, laser pulse sync signal is counted by the FPGA control module from zero. The moment the rising edge of the photon arrival timing signal is detected, the count value $N_n^{(i\,j)}$ at this time is saved as the coarse time of arrival photon. The time interval $t_n^{(i\,j)}$ between arrival photon and the nearest coming laser pulse sync signal is measured by the TCSPC module as the fine time of arrival photon. When the FPGA control module is used for first photon imaging, the first two photons imaging, etc., the rotation of the mirrors is controlled by the number of arrival photons per pixel, thereby changing the dwell time of the laser of each pixel. A threshold is set to prevent the dwell time from being too long. Taking the first photon imaging as an example, when the number of arrival photons of current pixel is 1 and the rising edge of the laser pulse sync signal is detected, or when the number of arrival photons of current pixel is 0 but the dwell time T_{pix} is equal to the setting threshold, the pixel scan sync signal is generated. When the rising edge of the pixel scan sync signal is detected, the X-axis galvo deflection signal and the Y-axis galvo deflection signal are synchronously output to dual-axis galvo to let the laser pulses reach the next pixel.

Single-photon counting imaging and the first photon imaging are integrated to achieve a wider range of applications. Under the extremely weak condition, the first photon imaging can be used

for efficient imaging, and when the light is relatively strong, single-photon counting imaging can be used to obtain better imaging results. The FPGA control module is combined with the TCSPC module to achieve continuous measurement of arrival time of photons. The TCSPC module uses a 'reverse start-stop' configuration and the total number of time bins is T_{bin}, so the arrival times of the photon sequence in pixel (i,j) are determined as:

$$T_n^{(i,j)} = \left(N_n^{(i,j)} + \frac{\left(T_{bin} - 1 - t_n^{(i,j)} \right)}{T_{bin}} \right) \times T_{laser} \quad n = 1, 2, 3, \ldots \tag{1}$$

3. Reconstruction of Reflectivity and Depth Image

3.1 Statistical Model of Detected Photon

The statistical model of photon that detected by the SPAD detector is built based on the doubly stochastic Poisson point processes. We assume that the intensity of each pulse emitted by the laser is constant and the number of photons is I. The laser emits a picosecond laser pulse, which then passes through the emission optical path and atmosphere to the pixel (i, j) of object surface, the number of photons that have not been reflected is $I_a = I\tau_a\eta_{em}$, τ_a is the laser single-pass transmittance in the atmosphere, η_{em} is the emission optical path efficiency. When the I_a photons reaches the surface of the object, the probability that m_{ij} photons is reflected can be subject to a binomial distribution:

$$P(X = m_{ij}) = C_{I_a}^{m_{ij}} (1 - R_{ij})^{I_a - m_{ij}} (R_{ij})^{m_{ij}} \tag{2}$$

Where R_{ij} is the reflectivity of pixel (i,j). When $I_a \to \infty$, the binomial distribution approaches a Poisson distribution. The Poisson distribution expression is:

$$\lim_{I_a \to \infty} C_{I_a}^{m_{ij}} (1 - R_{ij})^{I_a - m_{ij}} (R_{ij})^{m_{ij}} = \frac{\lambda_{ij}^{m_{ij}}}{m_{ij}!} e^{-\lambda_{ij}} \tag{3}$$

Where $\lambda_{ij} = I_a R_{ij}$ represents the average number of photons reflected by pixel (i,j) when it receives a laser pulse. After the reflected photons pass through the atmosphere, the average number of photons reaching the dual-axis galvo is $\lambda'_{ij} = \frac{\lambda_{ij}\tau_a \cos\theta_{ij}}{\pi}$, θ_{ij} is the angle between the incident laser and the normal to the object surface at pixel (i,j). Assume that the effective optical receiving area is Ar, the horizontal distance between the object and the dual-axis galvo is d_0, so the solid angle of the area to the object is $\Omega r = \frac{Ar}{d_0^2}$. After the reflected photons reach the single-photon detector, the photoelectrons are generated with the probability of the quantum efficiency η. The probability that the detector outputs n_{ij} single-photon pulses can be expressed as Poisson process:

$$P(X = n_{ij}) = \frac{L_{ij}^{n_{ij}}}{n_{ij}!} e^{-L_{ij}} \tag{4}$$

$$\begin{aligned} L_{ij} &= \eta\lambda'_{ij}\eta_{ec}\Omega r \\ &= \frac{\eta I \tau_a^2 R_{ij} \cos\theta_{ij} Ar \eta_{em}\eta_{ec}}{\pi d_0^2} \\ &= \frac{IR_{ij}\cos\theta_{ij}}{d_0^2} \times \frac{\tau_a^2 Ar\eta\,\eta_{em}\eta_{ec}}{\pi} \\ &= \frac{CIR_{ij}\cos\theta_{ij}}{d_0^2} \end{aligned} \tag{5}$$

Where L_{ij} is the average number of pulses that output by the detector of pixel (i,j) when it receives a laser pulse, $C = \frac{\tau_a^2 A\, r\eta\eta_{em}\eta_{ec}}{\pi}$ represents a constant. According to the principle of TCSPC technique, if a laser pulse reflects two or more photons, the TCSPC only records the first detected photon in

the laser pulse. That is, for one laser pulse, only two cases in which a photon is detected and no photons are detected can be distinguished. When a laser pulse arrives, according to formula (4), the probability that no photons are detected in pixel (i,j) is:

$$\begin{aligned} P(X=0) &= \frac{L_{ij}^{n_{ij}}}{n_{ij}!} e^{-L_{ij}} \\ &= e^{-L_{ij}} \\ &= e^{-\left(\frac{CIR_{ij}\cos\theta_{ij}}{d_0^2}\right)} \end{aligned} \tag{6}$$

The system emits N laser pulses for each pixel is assumed. The probability that k_{ij} photons are detected in pixel (i,j) is:

$$P(X=k_{ij}) = C_N^{k_{ij}} \left(1 - e^{-\left(\frac{CIR_{ij}\cos\theta_{ij}}{d_0^2}\right)}\right)^{k_{ij}} \left(e^{-\left(\frac{CIR_{ij}\cos\theta_{ij}}{d_0^2}\right)}\right)^{N-k_{ij}} \tag{7}$$

Similarly, when $N \to \infty$, the binomial distribution approaches Poisson distribution:

$$\lim_{N\to\infty} C_N^{k_{ij}} \left(1 - e^{-\left(\frac{CIR_{ij}\cos\theta_{ij}}{d_0^2}\right)}\right)^{k_{ij}} \left(e^{-\left(\frac{CIR_{ij}\cos\theta_{ij}}{d_0^2}\right)}\right)^{N-k_{ij}} = \frac{W_{ij}^{k_{ij}}}{k_{ij}!} e^{-W_{ij}} \tag{8}$$

according to formula (8):

$$W_{ij} = N\left(1 - e^{-\left(\frac{CIR_{ij}\cos\theta_{ij}}{d_0^2}\right)}\right) \tag{9}$$

From the formula (8) deduced above, it can be seen that the number of photons detected per pixel obeys the Poisson distribution with parameter W_{ij}. Therefore, the Poisson distribution parameter W_{ij} can be estimated by detecting the number of photons, and then the pixel reflectivity R_{ij} is obtained.

3.2 Time-Gated Filter

The pulse single output from SPAD detector includes not only single-photon pulses caused by the reflected photons from the object, but also the noise pulses caused by background photons and dark count of detector, therefore not all data of arrival times are used to estimate reflectivity and depth. In order to reduce the influence of dark count of the detector and most of background noise on reflectivity and depth imaging, we have adopted a time-gated filtering algorithm [30]. Different time thresholds are set depending on the pixels that the photons arrival. Photons whose TOF (the fine time of arrival photon in our system) is not within the setting threshold are determined as noise photons. The dual-axis galvo used in our system has an input analog position signal range of ± 10 V and three kinds of input mechanical position signal scale factors of 0.5 V/°, 0.8 V/° and 1 V/°. Take the input analog position signal voltage of ± 2.5 V and the input mechanical position signal scale factor of 0.5 V/° as an example: the maximum mechanical scan angle is $\theta_M = \pm 5^\circ$, the maximum optical scan angle is $\theta_o = \pm 10^\circ$ and the field of view (FOV) of receiver is $\theta_{FOV} = 10^\circ$. Assuming that the position of the 2D plane center of the scene where the objects are located is (0, 0). The resolution of reconstruct image is $r_1 \times r_2$ pixels, and light speed is c. The photon reaches the center position of pixel (i,j) as (p_x, p_y):

$$\begin{cases} p_y = \frac{d_0 \tan 10^\circ}{r_1/2} \times \left(\frac{r_1}{2} - i + \frac{1}{2}\right) \\ p_x = \frac{d_0 \tan 10^\circ}{r_2/2} \times \left(j - \frac{r_2}{2} - \frac{1}{2}\right) \end{cases} \tag{10}$$

The time threshold Δt_{ij} at the pixel (i,j) is:

$$\Delta t_{ij} = 2\frac{\sqrt{p_x^2 + p_y^2 + d_0^2}}{c} \tag{11}$$

3.3 Estimation Algorithm of Reflectivity and Depth

The maximum likelihood estimation method is used to estimate the parameter W_{ij} in formula (8), and then the estimation value of reflectivity of a pixel can be obtained according to formula (9). Take one pixel as an example, and regardless of the angle θ_{ij} between the incident laser and the normal to the object surface at pixel (i,j), the specific steps are as follows: (1) The scan time $[0, T_{pix}]$ corresponding to the pixel is divided into n equal parts, each aliquot is T. The number of photons X_1, $X_2, \ldots X_n$ detected by the pixel in each aliquot T can be regarded as independent random variables with a same distribution. A set of the measured photon counts $x_1, x_2, \ldots x_n$ can be regarded as a set of observations for random variables $X_1, X_2, \ldots X_n$. (2) The number of photons W detected in T can be estimated by maximum likelihood estimation method:

$$P(X_1 = x_1, X_2 = x_2, \ldots, X_N = x_n) = \prod_{h=1}^{n} \frac{W^{x_h}}{x_h!} e^{-W} = L(x_1, \ldots, x_n; W) \tag{12}$$

$$lnL(x_1, \ldots, x_n; W) = \sum_{h=1}^{n} x_h \ln W - nW - \ln\left(\prod_{h=1}^{n} x_h!\right) \tag{13}$$

Make $\frac{\partial \ln L(x_1,\ldots,x_n;W)}{\partial W} = \frac{\sum_{h=1}^{n} x_h}{W} - n = 0$, the maximum likelihood estimate of the photons' number detected in time T can be obtained:

$$\hat{W} = \frac{1}{n}\sum_{h=1}^{n} X_h \tag{14}$$

(3) Because of $E(\hat{W}) = E(\frac{X_1+X_2+\cdots+X_n}{n}) = W$, so $\frac{1}{n}\sum_{h=1}^{n} X_h$ is an unbiased estimator of W, and it's estimation error:

$$\Delta = \frac{MSE(\hat{W})}{W^2} = \frac{D(\hat{W})}{W^2} = \frac{1}{nW} \tag{15}$$

(4) In summary, the maximum likelihood estimation of W_{ij} for pixel (i,j) is the mean of the number of photons detected over multiple equal time T. So the maximum likelihood estimate of the reflectivity of the pixel (i,j) is:

$$R_{ij} = \frac{[\ln(N) - \ln(N - W_{ij})]d_0^2}{CI} \tag{16}$$

The photon measured by the TCSPC module is not the first photon of the emitted laser pulse, but the first detected photon by the detector. In addition, due to the time jitter of the dual-axis galvo, photon arrival timing signal and TCSPSC module, the fine time of the arrival photon in a pixel is floating. Depth estimation mainly uses centroid algorithm (CA) [29], Gaussian fitting (GF) [31], [32], exponential broadening Gaussian fitting (EBGF) [33] and so on. The number of photons detected per pixel is very small due to imaging in extremely weak environments. Experiments have shown that the CA expressed by formula (17) can achieve better results. $y_{ijt_n^{(i,j)}}$ is the total number of photons from pixel (i,j) with the time bins of fine time $t_n^{(i,j)}$. T_{bin} is total number of time bins of the TCSPC module, The estimated value of fine time of arrival photons from pixel (i,j) can be expressed:

$$T_{ij} = \frac{\sum_{t_n^{(i,j)}=0}^{T_{bin}} t_n^{(i,j)} y_{ijt_n^{(i,j)}}}{\sum_{t_n^{(i,j)}=0}^{T_{bin}} y_{ijt_n^{(i,j)}}} \tag{17}$$

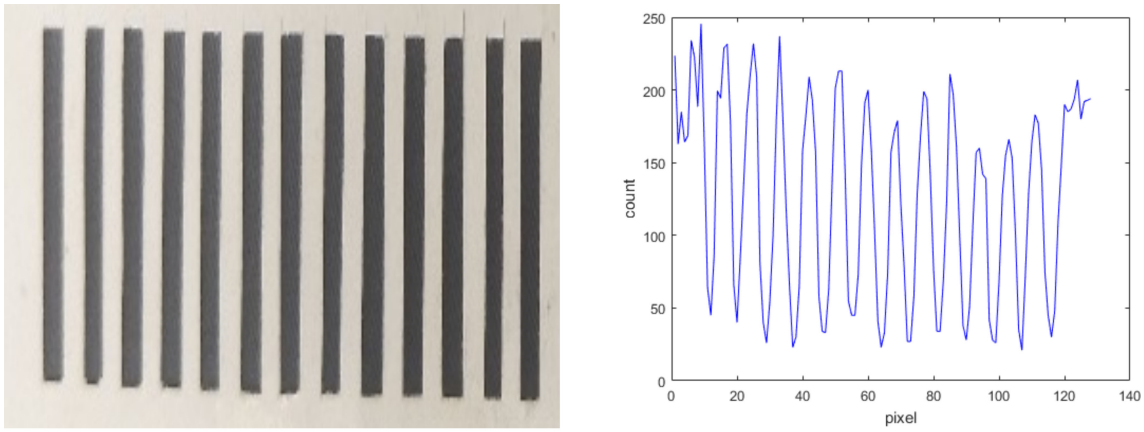

Fig. 3. The horizontal spatial resolution test. (a) Imaging object of a striped cardboard with a stripe pitch of 2 mm. (b) Plot of the counts statistics for each pixel with 128 pixels in all.

The depth D_{ij} of pixel (i,j) is expressed as:

$$D_{ij} = \frac{\left(T_{bin} - 1 - T_{ij}\right) \times T_{laser} \times c}{2T_{bin}} \tag{18}$$

4. Experiments and Discussions

4.1 Reflectivity Imaging Result

A stripe pitch of 2 mm of cardboard shown in Fig. 3(a) is used as an imaging object to measure the horizontal spatial resolution. When the laser frequency is set to 4 MHz, the resolution of the reflectivity image is set to 1 $\times$ 128 pixels, the scan time is set to 128 s (ie. the dwell time per pixel is 1 s), the Y-axis galvo is stabilized at the voltage zero point, and the X-axis galvo scans the object, the plot of the counts statistics for each pixel is shown in Fig. 3(b).

The diameter and divergence angle of the laser spot are the main factors that affecting the horizontal spatial resolution. The imaging distance in our experiment was only 1.5 m, so the effect of the divergence angle was small. From Fig. 3(b), the horizontal spatial resolution is 2 mm, which is only limited by the laser spot diameter of 2 mm. In this experiment, Total count value is 3226650, and when the time-gated filter is added, the effective photon count is 1371332, so SNR of the experiments is 73.9%.

When the laser frequency is set to 4 MHz, and the scan time is set to 384 s (ie. the dwell time at each pixel is 1.465 ms). The reflectivity and depth imaging with resolution of 512 $\times$ 512 pixels for the three scenes are shown in Fig. 4. The three scenes are: (1) Select a human head mold ($\approx$15 $\times$ 20 $\times$ 18 cm in W $\times$ H $\times$ D when viewed from the front) as a natural scene for a single object. (2) Choose cardboard of the letters ($\approx$15 $\times$ 12 cm in W $\times$ H) “N”, “C” and “U” as a simple scene for multiple objects. The longitudinal separation between letters “N” and “C” is 20 cm, and the longitudinal separation between letters “C” and “U” is 25 cm. (3) Pick a human head mold, small monster ($\approx$15 $\times$ 20 $\times$ 12.5 cm in W $\times$ H $\times$ D) and ceramic cup ($\approx$9 $\times$ 9.5 $\times$ 9 cm in W $\times$ H $\times$ D without the handle of the cup) as a complex natural scene with multiple objects, and the surface of the ceramic cup is affixed with the letters “NCU” ($\approx$5 $\times$ 1.65 cm in W $\times$ H) and the school badge of Nanchang University (the diameter is 5 cm). The longitudinal separation between the head mold and the small monster is 15 cm, and the longitudinal separation between the small monster and the ceramic cup is 8 cm.

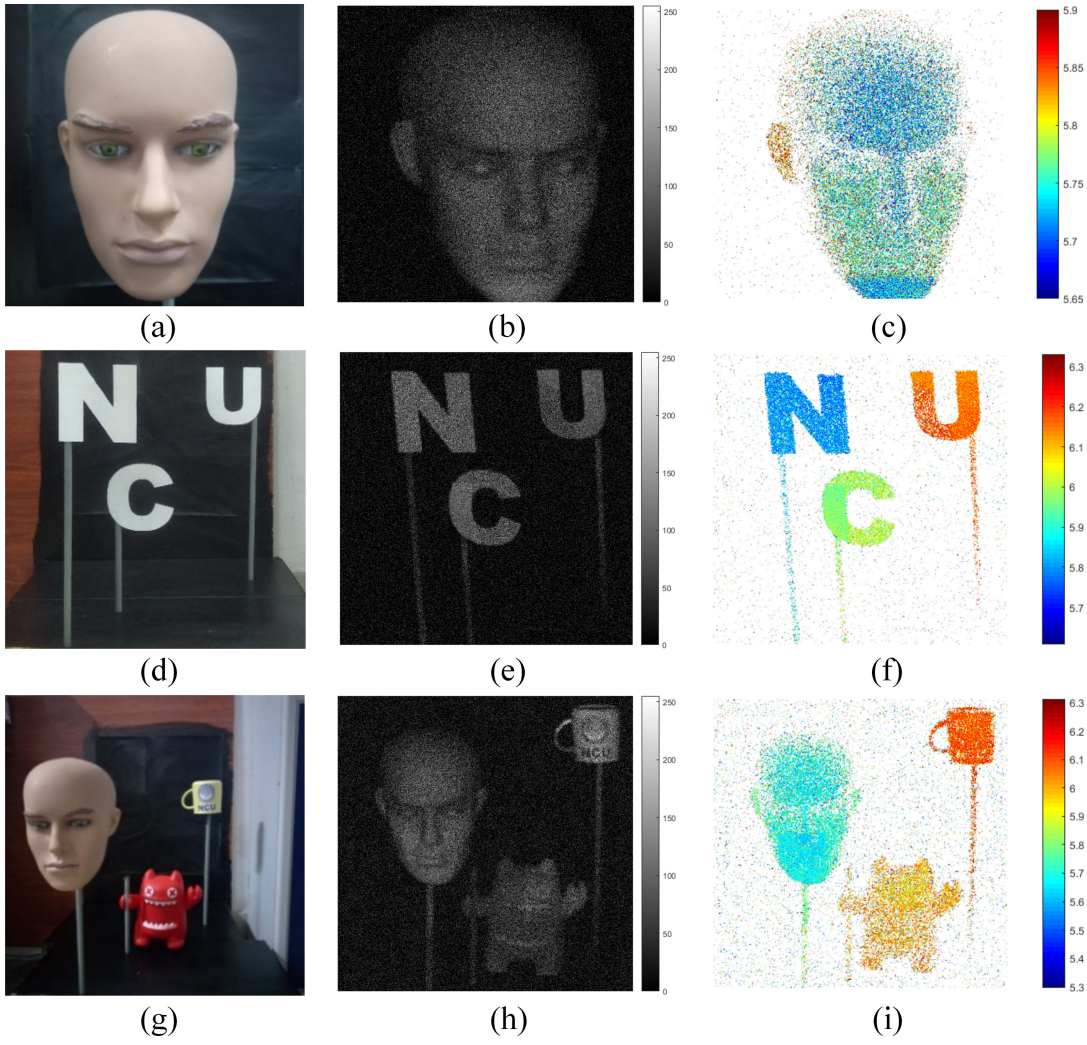

Fig. 4. Reflectivity and depth imaging results of different objects. (a) Photograph of a human head mold. (b) Reflectivity image of the human head mold with a resolution of 512 × 512 pixels. (c) Depth image of the human head mold with a resolution of 512 × 512 pixels. (d) Photograph of cardboard of the letters “N”, “C” and “U”. (e) Reflectivity image of the cardboard resolution of 512 × 512 pixels. (f) Depth image of the cardboard cutouts with a resolution of 512 × 512 pixels. (g) Photograph of a complex natural scene (h) Reflectivity image of the complex natural scene with a resolution of 512 × 512 pixels. (i) Depth image of the complex natural scene with a resolution of 512 × 512 pixels. Note: The unit of the color bar of the depth image is meter.

In Fig. 4(b), (e), (h), the average number of photons per pixel is 1.299, 1.042, and 1.270, respectively. The objects in the scenes of the reflectivity images are identified, and the outline of the objects are clear. Especially in the Fig. 4(h), the small letters “NCU” attached to the ceramic cup is identified, and the circular outline of the school badge is clear. Because of the horizontal spatial resolution is 2 mm, the school badge pattern is too densely packed, and the filling pitch is less than 2 mm, so the system does not recognize the pattern of the school badge.

4.2 Depth Imaging Result

In order to measure the depth resolution of our system, a reflector is used as an object for ranging experiment. When the laser frequency is set to 4 MHz, the scan time is set to 1 minute, and the

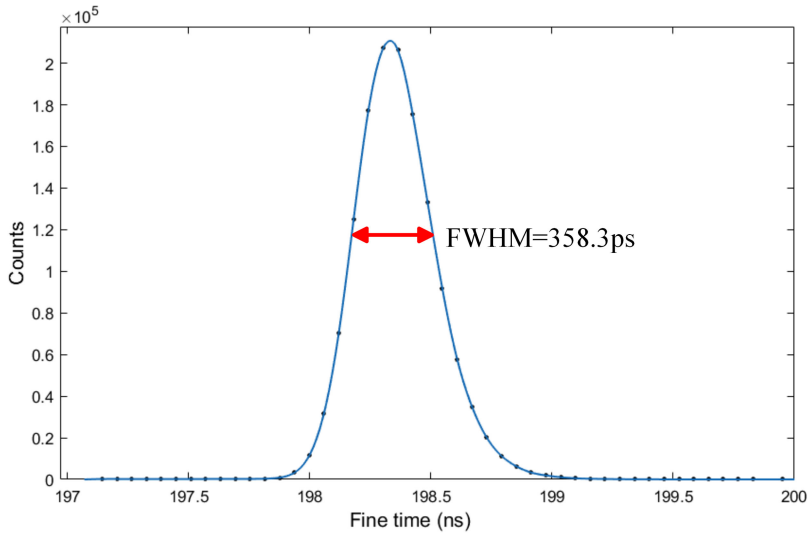

Fig. 5. Plot of depth resolution of ranging overlaid with fitted curve.

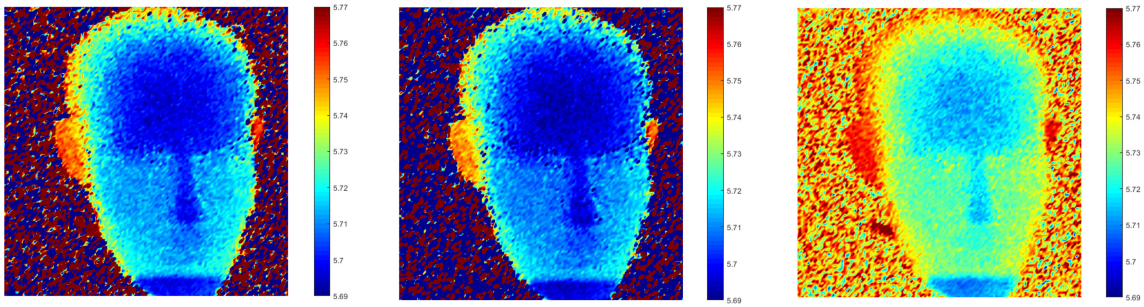

Fig. 6. The depth imaging results using different estimation algorithms. (a) Depth images of 128 × 128 pixels reconstructed by GF. (b) Depth images of 128 × 128 pixels reconstructed by EBGF. (c) Depth images of 128 × 128 pixels reconstructed by CA. Note: The unit of the color bar of the depth image is meter.

dual-axis galvo is fixed at an angle, the plot of depth resolution of ranging overlaid with fitted curve is shown in Fig. 5. The full width at half-maximum (FWHM) of the curve is 358.3 ps, that is to say, the corresponding depth resolution of the system is calculated to be 5.375 cm. So the FWHM is bigger than laser pulse width of 100 ps is due to total time jitter of the system. If the time jitter of the dual-axis galvo is Δt_{galvo}, the time jitter of the TCPSC module is Δt_{TCSPC} and the time jitter of the detector is Δt_{SPAD}, the total time jitter of the system is:

$$\Delta T = \sqrt{\Delta t_{galvo}^2 + \Delta t_{TCSPC}^2 + \Delta t_{SPAD}^2} \tag{19}$$

As shown in Fig. 4(c), (f), (i), the depth images constructed by CA can accurately recovers the 3D structure of the objects in the scene. Since the depth differences among the mouth, cheek and eyes are less than 1 cm, it is impossible to distinguish them in the depth image according to the depth resolution measured above. The depth imaging results with different estimation methods are shown in Fig. 6. The depth estimation of three pixels respectively located at forehead, cheeks and mouth using the three different algorithms are shown in Fig. 7. When there are many photons in a pixel, the depth calculated by GF and EBGF is very close. We can see better depth imaging results

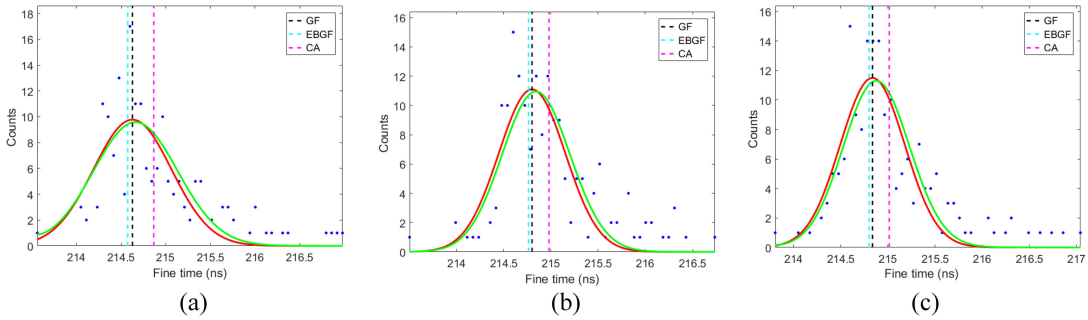

Fig. 7. The depth estimation of three different pixels using the three different algorithms. (a) Pixel located at forehead (b) Pixel located at cheeks. (c) Pixel located at mouth. Discrete points represent counting statistics of the fine time of arrival photons in our system. The three vertical dashed lines represent the estimated values by GF, EBGF, and CA, respectively. The two curves are fitted by GF and EBGF, respectively.

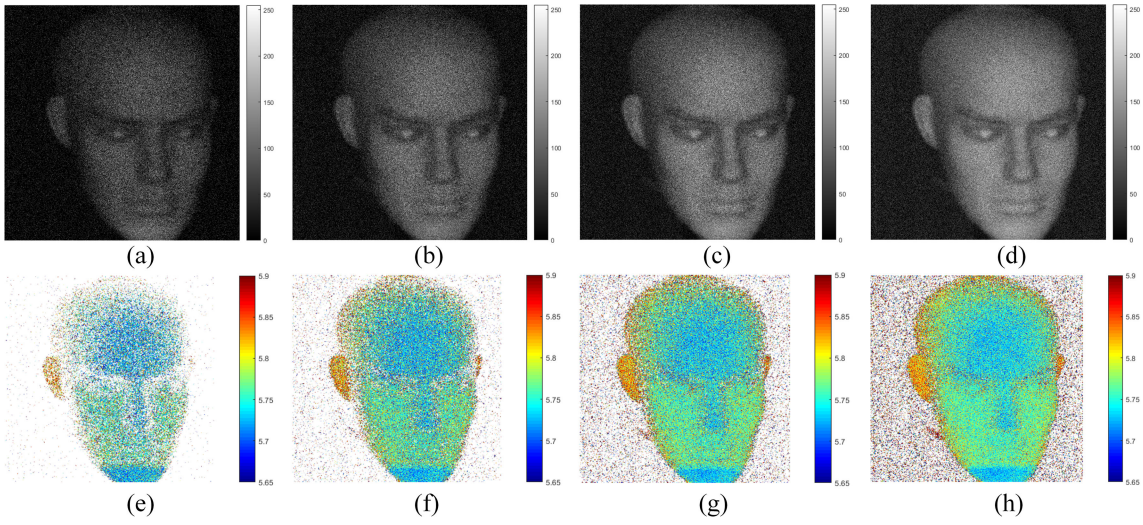

Fig. 8. The reflectivity and depth imaging results with different scan time. (a) Reflectivity imaging with scan time of 384s. (b) Reflectivity imaging with scan time of 768s. (c) Reflectivity imaging with scan time of 1152s. (d) Reflectivity imaging with scan time of 1536s. (e) Depth imaging with scan time of 384s. (f) Depth imaging with scan time of 768s. (g) Depth imaging with scan time of 1152s. (h) Depth imaging with scan time of 1536s. Note: The unit of the color bar of the depth image is meter.

and clearer outline obtained by GF and EBGF in Fig. 6. However, in other experimental results, it was found that when imaging time is very short or imaging is performed in an extremely weak lighting environment, the average number of photons detected by each pixel are extremely small (ie.1∼5), the depth image constructed by GF and EBGF are poor or even failed, and the better results can be obtained by CA.

4.3 Scan Time Versus Imaging Quality

When the laser frequency is set to 4 MHz and the imaging resolution is set to 512 $\times$ 512 pixels, reflectivity and depth imaging experiments were performed on the human head mold in different scan times, as shown in Fig. 8. The average photon number of each pixel of the Fig. 8(a), (b), (c), and (d) is 1.299, 2.590, 3.883, and 5.181, respectively. In reflectivity images, the facial features of the human head mold are more and more clear, and the phenomenon of specular highlights of the reflectivity images become more and more obvious. The depth information of the depth

images of the human head mold becomes more and more detailed. By increasing scan time, the reconstruction quality of reflectivity and depth images can be effectively improved. We analyze it according to formula (15), the more photons detected, the higher the estimation accuracy, and the less the influence of Poisson noise.

4.4 First Photon Imaging Results

According to equation (8), the photons received by the detector in a pixel (*i,j*) is a Poisson process with parameter W_{ij}. The probability distribution of k_{ij} photons detected during time t in a pixel (*i,j*) can be expressed as:

$$P(k_{ij}, t) = \frac{(W_{ij}t)^{k_{ij}}}{k_{ij}!}e^{-(W_{ij}t)} \tag{20}$$

In our design, the arrival time of photons in a pixel is continuously measured with a common starting point, that is, the rising edge of the pixel scan sync signal. The arrival time of the first photon T_1 is also a random variable. After pixel scan sync signal arrives, the probability distribution of no photons detected in [0, t) can be expressed as follows according to equation (20):

$$P(T_1 \geq t) = P(k_{ij} = 0, t) = e^{-W_{ij}t} \tag{21}$$

Therefore, the probability distribution function of the arrival time of the first photon of pixel (*i,j*) can be expressed as:

$$P(T_1 < t) = 1 - P(T_1 \geq t) = 1 - e^{-W_{ij}t} \tag{22}$$

The time interval T_n between the $(n-1)$-th photon and the n-th photon is also a random variable. The probability distribution function of T_n can be expressed as:

$$P(T_n < t) = 1 - P(T_n \geq t) = 1 - e^{-W_{ij}t} \tag{23}$$

where$P(T_n \geq t)$means the probability distribution function of no photon detected in $[t_{n-1}, t_{n-1} + t)$. By deriving equation (23), the probability density function of time interval of T_n can be written as:

$$f_{T_n} = W_{ij}e^{-W_{ij}t} \tag{24}$$

Equation (24) is an exponential distribution expression and the maximum likelihood estimation of W_{ij} is:

$$W_{ij}=\frac{n}{t_1 + t_2 + t_3 + \ldots t_n} \tag{25}$$

Where n represents the number of photons received by the detector in a pixel (*i,j*), and $t_1 + t_2 + t_3 + \ldots t_n$ represents the sum of n number of time intervals of arrival photon. In our experiment system, laser pulses are continuously emitted to one pixel of the imaging object, and then all the photon arrival times reflected by the pixel are measured with a common starting point, that is the rising edge of the pixel scan sync signal. Therefore, according to equation (1), $t_1 + t_2 + t_3 + \ldots t_n = T^{(i,j)}{}_n$, so formula (25) can be rewritten as:

$$W_{ij}=\frac{n}{T_n^{(i,j)}} \quad n = 1, 2, 3 \ldots \tag{26}$$

And then the reflectivity of the pixel (*i,j*) can be calculated by equation (16). That is to say, the reflectivity of each pixel is estimated by using the arrival time of the first photon of this pixel, thereby achieving first photon imaging. The arrival time of the first photon $T_1^{(i\,j)}$ composed of coarse time $N_1^{(i\,j)}$ and fine time $t_1^{(i\,j)}$. $N_1^{(i\,j)}$ is count value of laser pulse sync signal before receiving the first photon. In 'first-photon imaging' method first proposed by A. Kirmani *et al.* [25], the intensity of the light of each pixel is detected by recording the number of laser pulses that have been emitted. Because the fine time is much smaller than the coarse time, it has no effect on the imaging results. So the first photon imaging using our method is the same as the one proposed by A. Kirmani *et al.* In

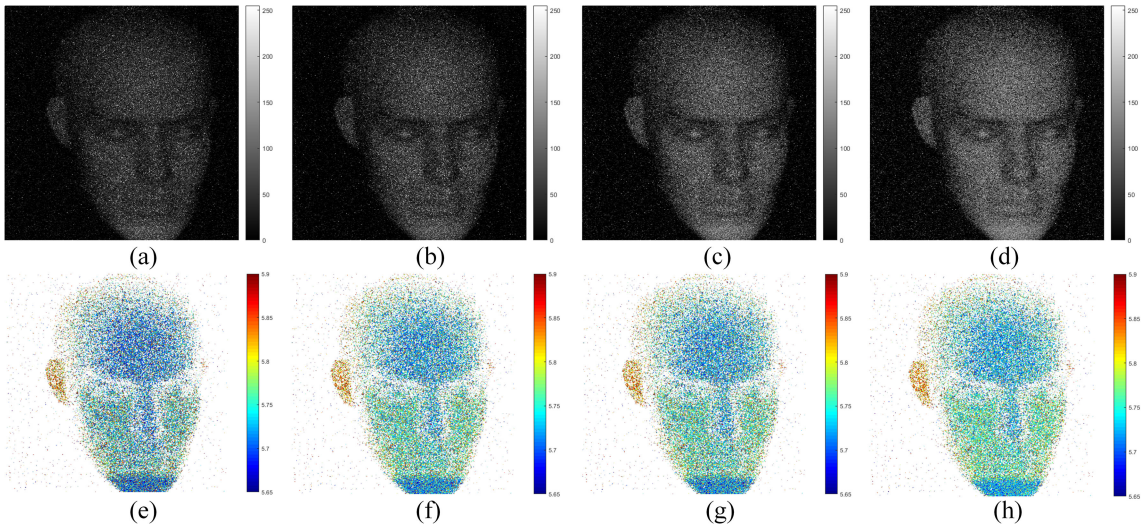

Fig. 9. The reflectivity and depth imaging results with different number of first photons. (a) Reflectivity imaging of the first photon. (b) Reflectivity imaging of the first two photons. (c) Reflectivity imaging of the first three photons. (d) Reflectivity imaging of the first four photons. (e) Depth imaging of the first photon. (f) Depth imaging of the first two photons. (g) Depth imaging of the first three photons. (h) Depth imaging of the first four photons. Note: The unit of the color bar of the depth image is meter.

addition, in our method, the reflectivity of each pixel can also be estimated by using the arrival time of the second or third, etc. photon of this pixel, thereby achieving first two photon imaging, first three photons imaging, etc.

When the laser frequency is set to 4 MHz, the imaging resolution is set to 512 $\times$ 512 pixels, the laser dwell time threshold is set to 1.465 ms, 2.930 ms, 4.395 ms and 5.860 ms for the first photon imaging, the first two photons imaging, the first three photon imaging, and the first four photon imaging respectively. The total scan time are 123.574 s, 218.619 s, 290.070 s and 455.471 s respectively. The images reconstructed according to formulas (22), (16) and (18) are shown in Fig. 9. Increasing the number of photons can reduce Poisson noise, so the reconstruction quality of the reflectivity and depth images can be effectively improved.

5. Conclusion

We proposed a continuous, high-precision method for measuring the arrival time of photons with a common starting point in a scanning position. On this basis, a reflectivity and depth imaging Lidar system is demonstrated. An FPGA control module is designed to control the dual-axis galvo to scan the objects, and synchronously record the coarse time of arrival photon and the arrival pixel of the photons. A TCSPC module is used to measure the fine time of arrival photon. A photon statistical model based on the doubly stochastic Poisson point processes, a time-gated filtering algorithm, and the reflectivity algorithm based on maximum likelihood estimation are derived. High-sensitivity reflectivity and depth imaging with 512 $\times$ 512 pixels are achieved. The experimental results show that the horizontal spatial resolution is 2 mm, the vertical depth resolution is 5.375 cm, and the average number of photons per pixel is less than 1.3 photons. When the imaging time is very short or the imaging is performed in a weak environment, the average number of photons detected by each pixel is extremely small, the depth image constructed by GF and EBGF are poor or even failed, and the better results can be obtained by CA. Increasing scan time can reduce Poisson noise, so the reconstruction quality of reflectivity and depth images can be effectively improved. Using the photon arrival time measurement method proposed in this paper, not only single-photon counting imaging but also first photon imaging, first two photons imaging, etc. can be realized.

References

[1] A. M. Pawlikowska, *Single-Photon Counting Lidar for Long-Range Three-Dimensional Imaging*. Edinburgh, U.K.: Heriot-Watt Univ., 2016.
[2] K. Tatsumi, T. Imai, and Y. Kawamura, "Atmospheric observation by airborne lidar using a Si-APD single-photon counting module," *Proc. SPIE*, vol. 3494, pp. 286–295, 1998.
[3] G. Buller and R. Collins, "Single-photon generation and detection," *Meas. Sci. Technol.*, vol. 21, 2009, Art. no. 012002.
[4] G. Gol'Tsman *et al.*, "Picosecond superconducting single-photon optical detector," *Appl. Phys. Lett.*, vol. 79, pp. 705–707, 2001.
[5] H. Dautet *et al.*, "Photon counting techniques with silicon avalanche photodiodes," *Appl. Opt.*, vol. 32, pp. 3894–3900, 1993.
[6] J. J. Degnan *et al.*, "Design and performance of a 3D imaging photon-counting microlaser altimeter operating from aircraft cruise altitudes under day or night conditions," *Proc. SPIE*, vol. 4546, pp. 1–11, 2002.
[7] M. McGill, D. Hlavka, W. Hart, V. S. Scott, J. Spinhirne, and B. Schmid, "Cloud physics lidar: Instrument description and initial measurement results," *Appl. Opt.*, vol. 41, pp. 3725–3734, 2002.
[8] Y. Yang, A. Marshak, S. P. Palm, T. Várnai, and W. J. Wiscombe, "Cloud impact on surface altimetry from a spaceborne 532-nm micropulse photon-counting lidar: System modeling for cloudy and clear atmospheres," *IEEE Trans. Geosci. Remote Sens.*, vol. 49, no. 12, pp. 4910–4919, Dec. 2011.
[9] Y.-h. Hu, J.-y. Wang, and Y.-q. Xue, "The waveform digitization of laser return in airborne laser remote sensing imaging," *J. Remote Sens.-Beijing*, vol. 5, pp. 110–113, 2001.
[10] P. A. Hiskett, C. S. Parry, A. McCarthy, and G. S. Buller, "A photon-counting time-of-flight ranging technique developed for the avoidance of range ambiguity at gigahertz clock rates," *Opt. Exp.*, vol. 16, pp. 13685–13698, 2008.
[11] A. McCarthy, R. J. Collins, N. J. Krichel, V. Fernández, A. M. Wallace, and G. S. Buller, "Long-range time-of-flight scanning sensor based on high-speed time-correlated single-photon counting," *Appl. Opt.*, vol. 48, pp. 6241–6251, 2009.
[12] D. O'Connor, *Time-Correlated Single Photon Counting*. New York, NY, USA: Academic, 2012.
[13] G. Buller and A. Wallace, "Ranging and three-dimensional imaging using time-correlated single-photon counting and point-by-point acquisition," *IEEE J. Sel. Topics Quantum Electron.*, vol. 13, no. 4, pp. 1006–1015, Jul./Aug. 2007.
[14] A. Spinelli, L. Davis, and H. Dautet, "Actively quenched single-photon avalanche diode for high repetition rate time-gated photon counting," *Rev. Sci. Instrum.*, vol. 67, pp. 55–61, 1996.
[15] M. Moeller *et al.*, "A four-wavelength multi-channel scanning time-resolved optical mammograph," in *Proc. Eur. Conf. Biomed. Opt.*, 2003, pp. 5138–5290.
[16] Y. Chen, J. D. Müller, P. T. So, and E. Gratton, "The photon counting histogram in fluorescence fluctuation spectroscopy," *Biophysical J.*, vol. 77, pp. 553–567, 1999.
[17] W. Becker, A. Bergmann, and C. Biskup, "Multispectral fluorescence lifetime imaging by TCSPC," *Microsc. Res. Techn.*, vol. 70, pp. 403–409, 2007.
[18] M. Henriksson, H. Larsson, C. Grönwall, and G. Tolt, "Continuously scanning time-correlated single-photon-counting single-pixel 3-D lidar," *Opt. Eng.*, vol. 56, 2016, Art. no. 031204.
[19] Z. Zhang *et al.*, "Ranging accuracy improvement of time-correlated signal-photon counting lidar," *Proc. SPIE*, vol. 10605, 2017, Art. no. 106050C.
[20] M. Henriksson, T. Olofsson, C. Grönwall, C. Brännlund, and L. Sjöqvist, "Optical reflectance tomography using TCSPC laser radar," *Proc. SPIE*, vol. 8542, 2012, Art. no. 85420E.
[21] A. McCarthy *et al.*, "Kilometer-range depth imaging at 1550 nm wavelength using an InGaAs/InP single-photon avalanche diode detector," *Opt. Exp.*, vol. 21, pp. 22098–22113, 2013.
[22] A. M. Pawlikowska, A. Halimi, R. A. Lamb, and G. S. Buller, "Single-photon three-dimensional imaging at up to 10 kilometers range," *Opt. Exp.*, vol. 25, pp. 11919–11931, 2017.
[23] Y. Kang, L. Li, D. Liu, D. Li, T. Zhang, and W. Zhao, "Fast long-range photon counting depth imaging with sparse single-photon data," *IEEE Photon. J.*, vol. 10, no. 3, Jun. 2018, Art no. 7500710.
[24] Q. Yan, B. Zhao, L. Sheng, and Y. a. Liu, "Continuous measurement of the arrival times of x-ray photon sequence," *Rev. Sci. Instrum.*, vol. 82, 2011, Art. no. 053105.
[25] A. Kirmani *et al.*, "First-photon imaging," *Sci.*, vol. 343, pp. 58–61, 2014.
[26] A. Kirmani, D. Shin, D. Venkatraman, F. N. Wong, and V. K Goyal, "First-photon imaging: Scene depth and reflectance acquisition from one detected photon per pixel," in *Proc. IEEE Int. Conf. Comput. Vision*, 2013, pp. 449–456.
[27] J. L. Pezzaniti and R. A. Chipman, "Angular dependence of polarizing beam-splitter cubes," *Appl. Opt.*, vol. 33, pp. 1916–1929, 1994.
[28] H. Jiang *et al.*, "Polarization splitter based on dual-core photonic crystal fiber," *Opt. Exp.*, vol. 22, pp. 30461–30466, 2014.
[29] Q. Yan, B. Zhao, Z. Hua, Q. Liao, and H. Yang, "High-speed quantum-random number generation by continuous measurement of arrival time of photons," *Rev. Scientific Instrum.*, vol. 86, 2015, Art. no. 073113.
[30] J. Busck and H. Heiselberg, "Gated viewing and high-accuracy three-dimensional laser radar," *Appl. Opt.*, vol. 43, pp. 4705–4710, 2004.
[31] H. Küpper, M. Spiller, and F. C. Küpper, "Photometric method for the quantification of chlorophylls and their derivatives in complex mixtures: Fitting with Gauss-Peak spectra," *Analytical Biochemistry*, vol. 286, pp. 247–256, 2000.
[32] H.-W. Lee, H.-J. Park, J.-H. Lee, and M. Song, "Accuracy improvement in peak positioning of spectrally distorted fiber Bragg grating sensors by Gaussian curve fitting," *Appl. Opt.*, vol. 46, pp. 2205–2208, 2007.
[33] Y. Chen, K. Yang, and H.-L. Liu, "Self-adaptive multi-peak detection algorithm for FBG sensing signal," *IEEE Sensors J.*, vol. 16, no. 8, pp. 2658–2665, Apr. 2016.